Stability analysis of tunnel face considering the shape of excavation and reinforcement measures

Yin Jiang[a], Yueping Tong[b], Aohui Ouyang[c*], Fei Ye[d], Chang Liu[e], Xingbo Han[f], Wenbo Peng[g]

[a] Graduate Student, School of Highway, Chang'an University, Xi'an, 710064, China. E-mail: jiangyin@chd.edu.cn

[b] PH.D.Student, School of Highway, Chang'an University, Xi'an, 710064, China. E-mail: typ@chd.edu.cn

[c] PH.D. Student, Civil, Structural & Environmental Engineering, University College Cork, Cork, T12 YF78, Ireland(Corresponding author). E-mail: 121100255@umail.ucc.ie

[d] Professor, School of Highway, Chang'an University, Xi'an, 710064, China. E-mail: xianyefei@126.com

[e] PH.D. Student, School of Civil Engineering, Southwest Jiaotong University, Chengdu, 610000, China. E-mail: 2844049895@qq.com

[f] Professor, School of Highway, Chang'an University, Xi'an, 710064, China. E-mail: xingbo.han@chd.edu.cn

[g] Researcher, CCCC Second Highway Consultants Co., Ltd., Wuhan, 430056, China. E-mail: 15871744068@139.com

Abstract

In mountain tunnels, a series of advanced reinforcement measures are often employed to maintain the stability of the tunnel face, particularly in challenging geological conditions. However, there is a lack of design theories regarding the advanced support structure for uniquely shaped tunnel faces, necessitating further exploration. Based on the limit equilibrium method, this paper presents a derivation of the mechanical model for analyzing excavation face stability considering shape changes and bolts. Additionally, a design theory for horizontal glass fiber bolts in longitudinally inclined tunnel faces is established. The reinforcement effect of the pipe shed is further considered. Finally, the proposed model is validated, and parameter analysis is conducted to guide improved design practices.

Keywords: Tunnel engineering; Limit equilibrium method; Longitudinal inclined tunnel face; Face bolts; Pipe shed

1 Introduction

With the sustaining spread of highway networks, the environment faced by tunnels is becoming more and more complex and diverse, among which the particularly prominent problems include the stability problem of soft rock tunnel face (Ding et al., 2017). To reveal the excavation face's failure shape and mechanism, scholars have studied the key factors such as the size of the influence area, the shape of the disturbance area, the displacement and stress development of the stratum in front of the tunnel excavation face through many laboratory model experiments (Chambon et al., 1994; Takano et al., 2006; Kirsch, 2010). Furthermore, with the continuous maturity of numerical simulation technology, it is also widely used to study the relationship between stratum or design factors and limit support pressure (Vermeer et al., 2002; Ukritchon and Keawsawasvong, 2017; Alagha and Chapman, 2019). Based on the results of the above research, scholars have proposed various improved calculation methods of limit support pressure, mainly including the limit analysis method (Leca and Dormieux, 1990; Mollon et al., 2009) and limit equilibrium method (Anagnostou and Kovári, 1996; Murayama et al., 1966).

For mountain tunnels, the stability of the tunnel face often requires stratum reinforcement measures to balance, such as near-horizontal jet grouting piles, honeycomb arches, advanced grouting pipe sheds, drainage pipe sheds, or horizontal glass fiber bolts. Among these, the advanced glass fiber bolt reinforcement technology is the most common and has been widely used. It uses the horizontal long bolt to anchor the leading core soil, mainly relying on the bonding force of the grouting layer around the glass fiber bolt to provide horizontal support. Due to the complexity of the force of the bolt and the difficulty in defining the scope of advanced core soil, the design of the horizontal face bolt is mainly based on empirical analogy and numerical simulation (Oreste and Dias, 2012; Oreste, 2009; Li et al., 2015; Zhang et al., 2022). With the deepening of scholars' understanding of it, the theoretical design is becoming more and more mature. The design theory of face bolt based on the limit analysis method mainly considers further the resistance power generated by the face bolt to balance its external force power (Pan and Dias, 2017). The design theory of face bolt based on the limit equilibrium method mainly utilizes the upper load, self-weight load of the sliding wedge, the support force of bolts and the friction resistance of the stratum to carry out static balance, and then solve the density of the bolt required for the minimum supporting force (Anagnostou and Serafeimidis, 2007).

Different from the blasting excavation method used in hard rock strata, the excavation of soft soil or weak surrounding rock tunnels can be achieved by mechanical or manual excavation, so the shape of the excavation face can be controlled. When advanced glass fiber grouting bolt is used for reinforcing the advanced core soil, the New Italy Method usually tilts the excavation face forward to improve its stability (Ranjbarnia et al., 2016). At the practical level, in some tunnels in Britain, the Matsumoto Tunnel in Japan and the Shanwang Tunnel in China, the field has adopted the technology of longitudinal forward-tilting tunnel face or spherical tunnel face for construction (Guan and Zhao, 2011). Practice shows this technology can effectually improve the advanced core soil's stress condition, increase the tunnel face stability, and reduce construction risk. In terms of theoretical research, Zhao, Huang, and Wang solved the limit support pressure required by the tunnel excavation face when the shield tunnel is inclined upward and downward in the stratum (Zhao et al., 2017; Huang et al., 2019; Wang et al., 2020). The results indicate that the limit support pressure will decrease if the tunnel face is inclined forward. In addition, Weng et al., (2020) used centrifugal experiments and numerical simulations to prove the occurrence of this phenomenon further.

Therefore, the influence of tunnel face shape on its stability can't be ignored. In this paper, on the basis of the Wedge-prism model, the theoretical model of the tunnel face bolt, considering the shape of the excavation, is established using the slice method. Furthermore, the calculation method of minimum bolt density in the inclined tunnel face is proposed in two cases: the middle and exit sections of the tunnel. Then, the mechanical stability model of the inclined tunnel face reinforced by the pipe shed and face bolt is proposed. Finally, it is verified by comparing it with previous studies, and the influence of strata and design parameters are analyzed.

2 Limit equilibrium method for the different shape of tunnel face

Based on the Wedge-prism model, the sliding wedge after the reinforcement of the glass fiber horizontal bolt is mainly subjected to four forces to maintain the balance, including the active load: the vertical load on the upper part of the sliding wedge (V), the self-weight of the sliding wedge (dG) and the passive load: the horizontal arching effect of the stratum on the sliding wedge when it deforms into the tunnel (dT_s), the supporting effect produced by the bolt of the excavation face (vertical support force dT_{fb} and horizontal support force dS). When the shape of the excavation face changes, the change in the upper part of the sliding wedge will cause a corresponding increase in the unsupported length of the tunnel, resulting in an increase in the vertical load on the sliding wedge. In addition, the change in the shape of the face will further decrease the volume of the sliding wedge so that its weight will be reduced accordingly. When the tunnel face is inclined from upright to forward, the change of the area on both sides will also reduce the horizontal soil arching effect on both sides of the stratum. Finally, because the overlap length of the face bolt is certain, the change of the tunnel face will make the original unstressed bolt (all located inside the sliding wedge) begin to play its role (**Fig. 1**).

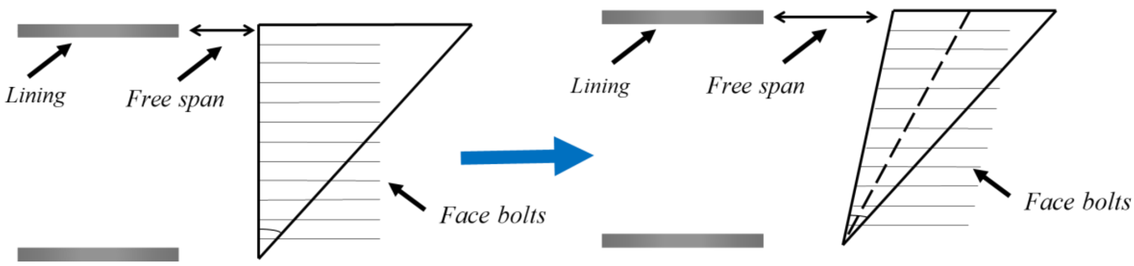

(a) Upright tunnel face (b) Inclined tunnel face

Fig. 1 Different shape of excavation face

Therefore, it is not difficult to find that the shape change of the tunnel face may increase or reduce its stability. Thus, Section 2 makes a theoretical feasibility analysis of this interesting phenomenon. First, we take a differential soil strip on the sliding wedge for analysis, as detailed in **Fig. 2**.

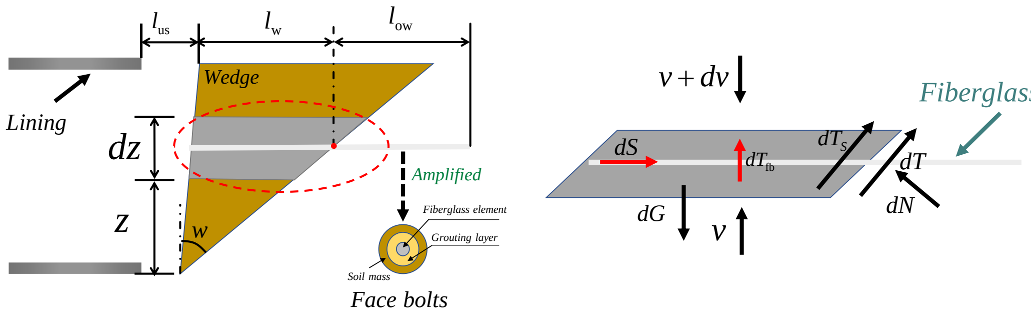

Fig. 2 Force of differential soil strip on excavation face after advanced pre-reinforcement (l_{us} is the unsupported span of the tunnel; l_w is the length of the glass fiber bolt inside the sliding wedge; l_{ow} is the length of the glass fiber bolt outside the sliding wedge; z is the distance from the soil slice to the bottom of the wedge; ω is the inclination angle of the wedge.)

When the shape of the tunnel face changes, the self-weight of the differential element (dG) can be expressed as:

$$dG = \gamma B\left(z\tan\left(w\right) - f\left(z\right)\right)dz \tag{1}$$

where γ is the weight of soil; B is the tunnel's width; $f(z)$ is the shape function of the tunnel face, which is related to the z; dz is the thickness of the differential element.

The relationship between tangential force (dT) and normal force (dN) on the sliding plane of the sliding wedge is:

$$dT = dN\tan\varphi \tag{2}$$

where φ is the internal friction angle of the soil.

After tunnel excavation, sliding wedge has a tendency to slide into the tunnel. At this time, the friction resistance provided by the strata on both sides of the sliding wedge is:

$$dT_s = 2\left(c + \lambda\sigma_{\text{soil}}\tan\varphi\right)\left(z\tan\left(w\right) - f\left(z\right)\right)dz \tag{3}$$

where c is the cohesion of soil.

From the above equation, we can observe that the horizontal soil arching effect in the stratum has changed. In particular, according to Terzaghi's loose earth pressure formula, the overlying stress of the strata on both sides of the differential element can be expressed as follows (Terazaghi, 1965):

$$\sigma_{\text{soil}}=\left[\frac{R\gamma-c}{\lambda\tan\varphi}(1-e^{-\lambda\tan\varphi\frac{c}{R}})+\sigma_{surf}e^{-\lambda\tan\varphi\frac{c}{R}}\right]\frac{(l_{us}'+H\tan\omega)}{z\tan(\omega)-f(z)} \tag{4}$$

where $R=\dfrac{B(l_{us}+H\tan\omega)}{2(B+l_{us}+H\tan\omega)}$; λ is the lateral pressure coefficient.

The unsupported length (l_{us}') after the change of excavation face is related to the shape of the face:

$$l_{us}'=f(H)+l_{us} \tag{5}$$

To simplify the calculation, here assumes that the cohesion of the face bolt can be fully utilized ($\tau_w=\tau_{max}$) and ignores the role of the bolt beam. The supporting force of the bolt on the sliding wedge can be expressed as:

$$dS(z)=s(z)Bdz=n\pi d_{hole}\cdot\min(\tau_w l_w,\tau_{ow}l_{ow})Bdz \tag{6}$$

where s is the support pressure; n and d_{hole} are the density and diameter of the face bolt, respectively; τ_w is the shear stress of bolts within the sliding wedge; τ_{ow} is the shear stress of bolts outside the sliding wedge.

In addition, the length of the internal and external bolts of the sliding wedge can be expressed as:

$$\begin{cases} l_w=z\tan(w)-f(z) \\ l_{ow}=l_{ol}+f(z)-z\tan(w) \end{cases} \tag{7}$$

According to the limit equilibrium method, the static equilibrium of differential element can be obtained:

$$\begin{cases} dT_s+dT+dS\sin\omega=(dV+dG)\cos\omega \\ dN=(dV+dG)\sin\omega+dS\cos\omega \end{cases} \tag{8}$$

Taking the Eq.s (1)-(7) into the Eq. (8), the linear non-homogeneous differential equation can be obtained by reorganizing:

$$B\frac{dV}{dz}-\Lambda V=M\left(\frac{z}{B}-\frac{f(z)}{B\tan(w)}\right)+P \tag{9}$$

where Λ, M, P are coefficients listed in Appendix I.

After solving, the maximum vertical load that the top of the sliding wedge can bear is :

$$V(z)=C_nB^3n\pi d_{\text{hole}}\tau_{\max}+C_cB^2c-C_\gamma B^3\gamma \tag{10}$$

Different from the case of the vertical tunnel face, the coefficients C_c and C_γ that determine the degree of cohesion and formation weight are expressed as follows:

$$C_c=\frac{C_v-1}{\Lambda}P_c+\left(\frac{F}{\Lambda^2}-\frac{C_v}{B^2\tan(w)}\int_0^z e^{\frac{-\Lambda z}{B}}f(x)dx\right)M_c \tag{11}$$

$$C_\gamma=\left(\frac{F}{\Lambda^2}-\frac{C_v}{B^2\tan(w)}\int_0^z e^{\frac{-\Lambda z}{B}}f(x)dx\right)M_\gamma \tag{12}$$

where C_v, P_c, F, M_c, M_γ are coefficients listed in Appendix I.

In addition, C_n determines the supporting effect of the bolt, which is closely related to its spatial location and layout. We need to discuss it in different situations:

The supporting effect provided by the bolt inside the sliding wedge can be expressed as:

$$C_{nw}=e^{\frac{\Lambda H}{B}}\cdot\int_0^H l_w B^{-2} e^{\frac{-\Lambda z}{B}}dz=e^{\frac{\Lambda H}{B}}\cdot\int_0^H \left(z\tan\left(\mathrm{w}\right)-f\left(z\right)\right)B^{-2}e^{\frac{-\Lambda z}{B}}dz \tag{13}$$

The supporting effect provided by the bolt outside of the sliding wedge can be expressed as:

$$C_{now}=e^{\frac{\Lambda H}{B}}\cdot\int_0^H l_{ow} B^{-2} e^{\frac{-\Lambda z}{B}}dz=e^{\frac{\Lambda H}{B}}\cdot\int_0^H \left(l_{ol}-z\tan\left(\mathrm{w}\right)+f\left(z\right)\right)B^{-2}e^{\frac{-\Lambda z}{B}}dz \tag{14}$$

When all the bolts are located inside the sliding wedge:

$$C_n=0 \tag{15}$$

However, which part of the tunnel face bolt provides the support function needs to be discussed in combination with $f(z)$ and w.

3 Bolt design theory of longitudinal inclined tunnel face

The contribution of tunnel face shape to its stability is complex. According to the Eq. (10), there is an optimal shape of the tunnel face in theory so that the bearing capacity of the sliding wedge can reach the maximum value. Although the complex shape of the tunnel face can improve its stability in the soft soil layer to a certain extent, it not only puts forward new requirements for the theoretical level of engineers but also challenges the operation difficulty and fineness of construction machinery. Considering the actual needs, we will discuss the longitudinal inclined tunnel face in this section.

3.1 Middle section of tunnel

When the soft soil tunnel enters the hole, the advanced bolts laid on the inclined tunnel face are usually equal in length. They will form a parallelogram in the stratum, as depicted in **Fig. 3**.

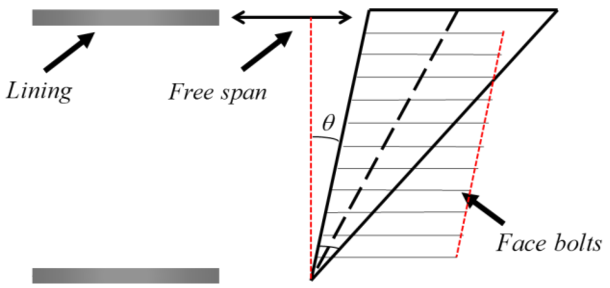

Fig. 3 Face bolts arrangement of inclined excavation face (middle section of tunnel)

At this time, the end connection line of bolts will be parallel to the tunnel face. We assume that the inclination angle of the tunnel face is θ, then the $f(z)$ can be further transformed into:

$$f\left(z\right)=z\tan\left(\theta\right) \tag{16}$$

However, we need to pay attention here that θ is constrained by the maximum unsupported length. If the forward inclination of the tunnel face is too large, resulting in the tunnel's unsupported length (l_{us}') exceeding its maximum value, the risk of roof collapse and block falling may occur. Therefore, in order to obtain the maximum possible inclination angle, let l_{us} = 0. According to the study of the maximum unsupported length (Anagnostou and Perazzelli, 2013; Anagnostou and

Perazzelli, 2015), the maximum inclination angle of the tunnel face is:

$$\theta_{\max} = \arctan\left(\frac{c}{\gamma H\left(0.5 - c/\gamma B\right)}\right) \tag{17}$$

After taking it into Eq. (11) and (12), it can be obtained:

$$C_\gamma = \left(\frac{F}{\Lambda^2} - \left(\frac{2BC_v}{\Lambda^3} - \left(\frac{2B}{\Lambda^3} + \frac{2H}{\Lambda^2} + \frac{H^2}{\Lambda B^2}\right)\right)\frac{\tan(\theta)}{\tan(w)}\right)M_\gamma \tag{18}$$

$$C_c = \frac{C_v - 1}{\Lambda}P_c + \left(\frac{F}{\Lambda^2} - \left(\frac{2BC_v}{\Lambda^3} - \left(\frac{2B}{\Lambda^3} + \frac{2H}{\Lambda^2} + \frac{H^2}{\Lambda B^2}\right)\right)\frac{\tan(\theta)}{\tan(w)}\right)M_c \tag{19}$$

At this time, C_n can be divided into three categories for discussion.

a) When w is very small, $w \le w_1 = \arctan\left(\frac{2z\tan(w) + 2l_{us} + l_{ol}}{2H}\right)$. At this time, the horizontal support effect will be completely provided by the bond force of the bolt inside the sliding wedge.

$$s_{wa}(z) = \int_0^H e^{\frac{-\Lambda z}{B}} n\pi d_{hole}\tau_{\max} z\left(\tan(w) - \tan(\theta)\right)dz \tag{20}$$

b) When w is moderate, $w_1 \le w \le w_2 = \arctan\left(\frac{z\tan(w) + l_{us} + l_{ol}}{H}\right)$. There may be two situations for the face bolt.

$$s(z) = \begin{cases} s_{wb}(z) = \int_0^H e^{\frac{-\Lambda z}{B}} n\pi d_{hole}\tau_{\max}\left(l_{ol} - z\tan(w) + z\tan(\theta)\right), z_1 < z \le H \\ s_{wa}(z) = \int_0^H e^{\frac{-\Lambda z}{B}} n\pi d_{hole}\tau_{\max} z\left(\tan(w) - \tan(\theta)\right)dz, z \le z_1 \end{cases} \tag{21}$$

where z_1 is the neutral height, and the length of the horizontal bolt inside the sliding wedge is equal to that outside, as depicted in **Fig. 3**. It can be expressed as:

$$z_1 = \frac{l_{ol}}{2\tan(w) - 2\tan(\theta)} \tag{22}$$

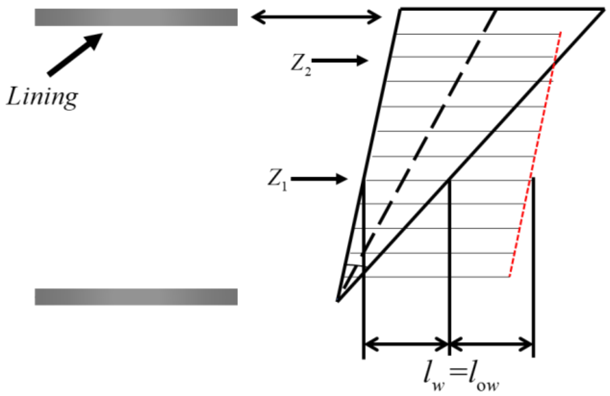

Fig. 4 Special height diagram

c) When w is too large, $w_2 \le w$. At this time, part of the horizontal bolt may be completely located inside the sliding wedge. The supporting force can be expressed as:

$$s(z)=\begin{cases} 0, z_2 < z \le H \\ s_{wb}(z)=\int_0^H e^{\frac{-\Lambda z}{B}} n\pi d_{hole}\tau_{\max}\left(l_{ol} - z\tan(w) + z\tan(\theta)\right), z_1 < z \le z_2 \\ s_{wa}(z)=\int_0^H e^{\frac{-\Lambda z}{B}} n\pi d_{hole}\tau_{\max} z\left(\tan(w) - \tan(\theta)\right) dz, z \le z_1 \end{cases} \tag{23}$$

where z_2 is the limiting height, and the length of the horizontal bolt inside the sliding wedge is equal to its overlap length, as depicted in **Fig. 3**. It can be expressed as:

$$z_2 = \frac{l_{ol}}{\tan(w) - \tan(\theta)} \tag{24}$$

At this time, C_{n1} is shown as :

$$C_{n1} = \frac{\mathrm{ps}}{\Lambda^2}\left(\tan(\mathrm{w}) - \tan(\theta)\right)\begin{cases} e^{\frac{\Lambda H}{B}} - 1 - \frac{\Lambda H}{B}, \ w \le w_1 \\ \mathrm{e}^{\frac{\Lambda H}{B}} - 2\mathrm{e}^{\left(\frac{\Lambda H}{B}\left(1+\frac{(\tan(\mathrm{w}_1)-\tan(\theta))}{(\tan(\mathrm{w})-\tan(\theta))}\right)\right)} + \left(1+\frac{\left(\tan(\mathrm{w}_2) - \tan(\theta)\right)}{\left(\tan(\mathrm{w}) - \tan(\theta)\right)}\right)\frac{\Lambda H}{B} + 1, \ \ w_1 < w \le w_2, \\ \left(e^{\frac{\Lambda H}{B}\frac{(\tan(\mathrm{w}_1)-\tan(\theta))}{(\tan(\mathrm{w})-\tan(\theta))}} - 1\right)^2, \ \ w_2 < w\,. \end{cases} \tag{25}$$

According to the boundary conditions, the bearing capacity of the sliding wedge is equal to the overlying loose soil pressure $V(H) = V_{\mathrm{Prism}}$, the required minimum bolt density can be obtained (Anagnostou and Perazzelli, 2015):

$$n_r = f_{1c} - f_{2c}\frac{c}{H} + f_{3c}\frac{\sigma_{\text{prism}}}{H} \tag{26}$$

where:

$$f_{1c} = \frac{C_\gamma \gamma}{\pi d_{\text{hole}} \tau_{\max} C_{n1}} \tag{27}$$

$$f_{2c} = \frac{C_c H}{\pi d_{\text{hole}} \tau_{\max} C_{n1} B} \tag{28}$$

$$f_{3c} = (\frac{H}{B})^2 \frac{\tan\omega}{\pi d_{\text{hole}} \tau_{\max} C_{n1}} \tag{29}$$

3.2 Exit section of tunnel

When the tunnel is out of the hole, the distribution of face bolt is trapezoidal. At this time, the end connection line of bolts is perpendicular to the tunnel axis, and the bolt exceeding the entrance position (the red line position below) will be in the air and can not play a role (**Fig. 5**).

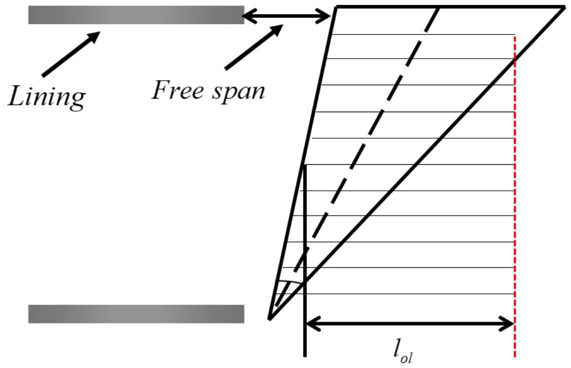

Fig. 5 Face bolts arrangement of inclined excavation face (exit section of tunnel)

Under this condition, the coefficient C_c related to the cohesion of the stratum and the coefficient C_γ related to the weight of the stratum soil remain unchanged, but C_n needs to be classified and discussed:

a) When $w \le w_1 = \arctan\left(\frac{l_{us}' + l_{ol}}{2H}\right)$, the horizontal support force is:

$$s_{wa}(z) = \int_0^H e^{\frac{-\Lambda z}{B}} n\pi d_{hole}\tau_{\max} z\left(\tan(w) - \tan(\theta)\right)dz \tag{30}$$

b) When $w_1 \le w \le w_2 = \arctan\left(\frac{l_{ol}}{H}\right)$, the horizontal support force is:

$$s(z) = \begin{cases} s_{wb}(z) = \int_0^H e^{\frac{-\Lambda z}{B}} n\pi d_{hole}\tau_{\max}\left(l_{ol} - z\tan(w) + z\tan(\theta)\right), z_1' < z \le H \\ s_{wa}(z) = \int_0^H e^{\frac{-\Lambda z}{B}} n\pi d_{hole}\tau_{\max} z\left(\tan(w) - \tan(\theta)\right)dz, z \le z_1' = \dfrac{l_{ol}}{2\tan(w) - 2\tan(\theta)} \end{cases}$$

(31)

c) When $w_2 \le w$, the horizontal support force is:

$$s(z)=\begin{cases} 0, z_2' = \dfrac{l_{ol}}{\tan(w)-\tan(\theta)} < z \le H \\ s_{wb}(z)=\int_0^H e^{\frac{-\Lambda z}{B}} n\pi d_{hole}\tau_{\max}\left(l_{ol}-z\tan(w)+z\tan(\theta)\right), z_1' < z \le z_2' \\ s_{wa}(z)=\int_0^H e^{\frac{-\Lambda z}{B}} n\pi d_{hole}\tau_{\max} z\left(\tan(w)-\tan(\theta)\right)dz, z \le z_1' \end{cases} \tag{32}$$

At this time, C_{n2} is shown as :

$$C_{n2}=\frac{ps\left(\tan(w)-\tan(\theta)\right)}{\Lambda^2}\begin{cases} e^{\frac{\Lambda H}{B}}-1-\dfrac{\Lambda H}{B}, \quad w \le w_1 \\ e^{\frac{\Lambda H}{B}}+\dfrac{\left(\tan(\theta)-2\tan(w)\right)}{\left(\tan(w)-\tan(\theta)\right)} e^{\frac{\Lambda H}{B}\left(1-\frac{2\tan(w_1)-\tan(\theta)}{2\tan(w)-\tan(\theta)}\right)} \\ +\dfrac{\tan(w)}{\left(\tan(w)-\tan(\theta)\right)}\left(\dfrac{\Lambda H}{B}+1\right) \\ -\dfrac{\tan(w_2)}{\left(\tan(w)-\tan(\theta)\right)}H, \quad w_1 < w \le w_2, \\ e^{\frac{\Lambda H}{B}}+\dfrac{\tan(w)}{\left(\tan(w)-\tan(\theta)\right)} e^{\frac{\Lambda H}{B}\left(1-\frac{\tan(w_2)}{\tan(w)}\right)} \\ +\dfrac{\left(\tan(\theta)-2\tan(w)\right)}{\left(\tan(w)-\tan(\theta)\right)} e^{\frac{\Lambda H}{B}\left(1-\frac{2\tan(w_1)-\tan(\theta)}{2\tan(w)-\tan(\theta)}\right)}, \quad w_2 < w . \end{cases} \tag{33}$$

According to the boundary conditions, the bearing capacity of the sliding wedge is equal to the overlying loose soil pressure $V(H)=V_{\text{Prism}}$, the required minimum bolt density can be obtained:

$$n_r = f_{1d} - f_{2d}\frac{c}{H} + f_{3d}\frac{\sigma_{\text{prism}}}{H} \tag{34}$$

where:

$$f_{1d} = \frac{\gamma C_\gamma}{\pi d_{\text{hole}}\tau_{\max} C_{n2}} \tag{35}$$

$$f_{2d} = \frac{C_c H}{\pi d_{\text{hole}}\tau_{\max} C_{n2} B} \tag{36}$$

$$f_{3d} = \left(\frac{H}{B}\right)^2 \frac{\tan\omega}{\pi d_{hole} \tau_{max} C_{n2}} \tag{37}$$

4 Bolt design theory of longitudinal inclined tunnel face under pipe shed

In the previous section, we discussed the possibility of longitudinally inclined tunnel face and the design density formula of the bolt under the corresponding two working conditions. However, one thing we must recognize is that the longitudinal inclined tunnel face is under an important premise, that is, the tunnel stratum can allow the tunnel face to tilt, and it is limited by the cohesion of the stratum. So for sandy soil, in order to achieve the possibility of an inclined tunnel face, it is necessary to pre-reinforce the vault through pipe shed, advanced small pipe or horizontal jet grouting pile. In this section, we established the design theory of face bolt with longitudinal inclined tunnel face under pipe shed assisted construction.

4.1 Mechanical model of pipe shed

Fig. 6 shows the excavation face reinforced by pipe shed and horizontal glass fiber bolt. In this composite reinforcement structure, the advanced horizontal bolt mainly bears the horizontal support function, while the pipe shed bears the vertical load from the stratum on the upper part of the sliding wedge. x_1 is the starting point of the pipe shed, located in the upper part of the lining structure; x_2 is the point on the pipe shed at the end of the lining; x_3 is the intersection point between the top of the inclined tunnel face and the pipe shed; x_4 is the intersection point between the sliding surface of the sliding wedge and the pipe shed; x_5 is the end point of the pipe shed. l_{sp} is the length of the pipe shed behind the lining; l_{us} is the unsupported length of the tunnel; l_{wu} is the length of the pipe shed at the top of the sliding failure zone; l_{owu} is the length of the pipe shed outside the sliding wedge.

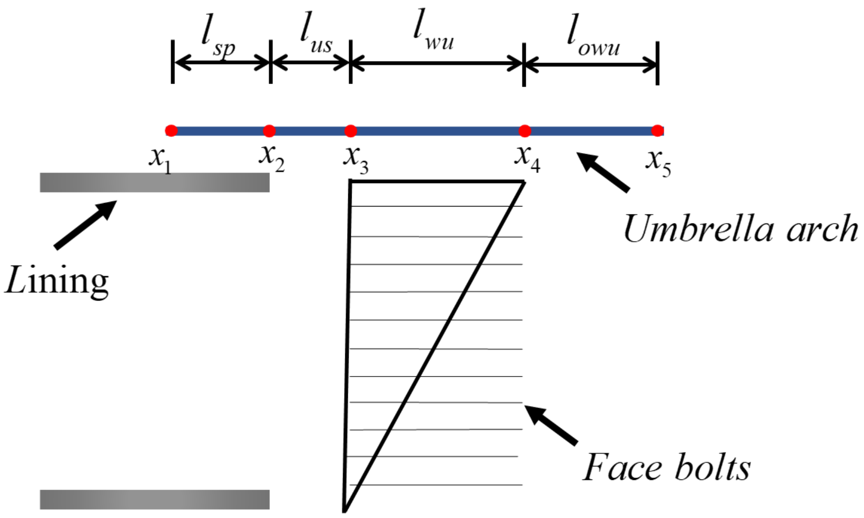

Fig. 6 Excavation face after pre-reinforcement of pipe roof and horizontal bolt

Considering that the pipe shed is mainly subjected to vertical load to produce deflection, it is assumed to be an elastic foundation beam for analysis. Specifically, the Winkler beam model is used (Zhang et al., 2020). Since the pipe shed is built between equal lengths and intervals, we take one of the pipe sheds for analysis. The pipe shed produces deflection under the action of an overlying load, which is mainly divided into four stages (**Fig. 6**).

a) l_{sp} section: The lining and the pipe shed above the lining jointly bear the bending moment and shear force of the pipe shed caused by the loose load on the excavation surface. And the pipe shed corresponding to point x_l is fixed. At this time, the mechanical model of the pipe shed of the l_{sp} section can be described as:

$$E_1 J_1 \cdot \frac{d^4 y_{\mathrm{sp}}(x)}{dx^4} + p_{\mathrm{sp}}(y) = 0 \tag{38}$$

where E_1 is the elastic modulus of each grouting rigid pipe; J_1 is the moment of inertia; $y_{\mathrm{sp}}(x)$ is the vertical displacement of the pipe shed point in the l_{sp} section above the lining; $p_{\mathrm{sp}}(y)$ is the foundation reaction force of the l_{sp} section pipe shed above the lining, which can be expressed as:

$$p_{\mathrm{sp}}(y) = k_{sp} d_{\mathrm{pipe}} y_{\mathrm{sp}}(x) \tag{39}$$

where d_{pipe} is the diameter of the pipe shed; k_{sp} is the foundation resistance coefficient of l_{sp} section, specifically:

$$k_{sp} = \frac{E_2\left(R_{eq}^2 - \left(R_{eq} - t\right)^2\right)}{R_{eq}\left(1+\mu_s\right)\left(\left(1-2\mu_s\right)R_{eq}^2 + \left(R_{eq}-t\right)^2\right)} \tag{40}$$

where E_2 is the elastic modulus of concrete; R_{ep} is the equivalent diameter of the tunnel, $R_{eq} = \dfrac{B+H}{4}$; t is the thickness of lining (primary support); μ_s is the Poisson's ratio of concrete.

b) l_{us} section: The pipe shed here is usually the most unfavourable section. There is no foundation reaction support at the lower part of the pipe shed, and the upper part directly bears the loose soil pressure load. The force is:

$$E_1 J_1 \cdot \frac{d^4 y_{\mathrm{us}}(x)}{dx^4} = V_{\mathrm{pipe}} \tag{41}$$

where $y_{\mathrm{us}}(x)$ is the vertical displacement of any point on the pipe shed of the l_{us} section ;

In addition, the vertical load on a pipe shed V_{pipe} is:

$$V_{\mathrm{pipe}} = \sigma_{\mathrm{vn}} l_s \tag{42}$$

where l_s is the spacing of the pipe shed; σ_{vn} is the vertical stress above the excavation face.

c) l_{wu} section: Here, the pipe shed is above the sliding wedge. The upper part of the pipe shed receives the loose soil pressure load of the failure zone, and the lower part is supported by the foundation reaction force provided by the sliding wedge. The mechanical behaviour can be described as follows:

$$E_1 J_1 \cdot \frac{d^4 y_{\mathrm{wu}}(x)}{dx^4} + p_{\mathrm{wu}}(y) = V_{\mathrm{pipe}} \tag{43}$$

where $y_{\mathrm{wu}}(x)$ is the displacement of any point of the l_{wu} pipe shed; the specific form of $p_{\mathrm{wu}}(y)$ is :

$$p_{\mathrm{wu}}(y) = k_{wu} d_{\mathrm{pipe}} y_{\mathrm{wu}}(x) \tag{44}$$

The foundation resistance coefficient k_{wu} of this section is:

$$k_{wu} = \frac{3E_3}{\left(1-\mu_{\mathrm{g}}\right)\left(5-6\mu_{\mathrm{g}}\right)R_{eq}} \tag{45}$$

where E_3 is the elastic modulus of the formation; μ_g is the Poisson's ratio of the formation.

d) l_{owu} section: This section is deep in the stable stratum and is not subjected to vertical load like l_{sp} section, but bears the bending moment transmitted by other sections.

$$E_1 J_1 \cdot \frac{d^4 y_{\mathrm{owu}}(x)}{dx^4} + p_{\mathrm{owu}}(y) = 0 \tag{46}$$

where $y_{\mathrm{owu}}(x)$ is the vertical displacement of the pipe shed in the l_{owu} section; the foundation reaction force $p_{\mathrm{owu}}(y)$ is expressed as :

$$p_{\mathrm{owu}}(y) = k_{wu} d_{\mathrm{pipe}} y_{\mathrm{owu}}(x) \tag{47}$$

To solve the displacement of the pipe shed in the above four stages, it is necessary to rely on 12 boundary conditions. The boundary equation and the vertical displacement expression of each stage are detailed in Appendix II. After solving the vertical displacement of any point, the shear force and bending moment on the pipe shed can be obtained.

4.2 Design theory of face bolt

The supporting mechanism of the pipe shed can be considered to bear the vertical load and reduce the vertical load of the self-weight failure zone of the sliding wedge through its force. However, when the tunnel face is inclined, not only the factors mentioned before (such as the force of the face bolt, and the weight of the sliding wedge) have changed, but also the force of the pipe shed itself has changed.

The length of the pipe shed in the l_{us} section can be described as:

$$l_{us} = f(H) = H\tan(\theta) = x_3 - x_2 \tag{48}$$

In order to maximize the tilt angle of the tunnel face, it is considered that the primary lining can be applied to the bottom of the tunnel face in time.

In addition, the length of the pipe shed in the l_{wu} section is decided by the θ and w.

$$l_{wu} = H\tan(w) - H\tan(\theta) = x_4 - x_3 \tag{49}$$

Finally, under the condition of fixing the length of pipe shed in the l_{sp} section, the length of the pipe shed in the l_{owu} section can be described as :

$$l_{owu} = l_p - l_{wu} - l_{us} - l_{sp} \tag{50}$$

where l_p is the overlap length of the pipe shed.

a) When the overlap length of the pipe shed is long enough, the length of the pipe shed (l_p) is much larger than the distance from the farthest vertex of the sliding wedge to the fixed end of the pipe shed (x_4 - x_1). At this time, as illustrated in **Fig. 7**, the vertical load of the sliding wedge after the pipe shed support is:

$$\sigma_{\mathrm{pipe}} = \frac{d_{\mathrm{pipe}} k_{\mathrm{g}} \int_{l_{\mathrm{sp}}+l_{\mathrm{us}}}^{l_{\mathrm{sp}}+l_{\mathrm{us}}+l_{\mathrm{wu}}} y_{\mathrm{wu}}(x)\,\mathrm{dx}}{l_{us}+l_{wu}} \tag{51}$$

After taking it into Eq. (26), it can be obtained that the required minimum bolt density is:

$$n_r = f_{1c} - f_{2c}\frac{c}{H} + f_{3c}\frac{d_{\text{pipe}}k_g\int_{x_3}^{x_4} y_{\text{wu}}(x)\,\text{dx}}{H(l_{us}+l_{wu})} \tag{52}$$

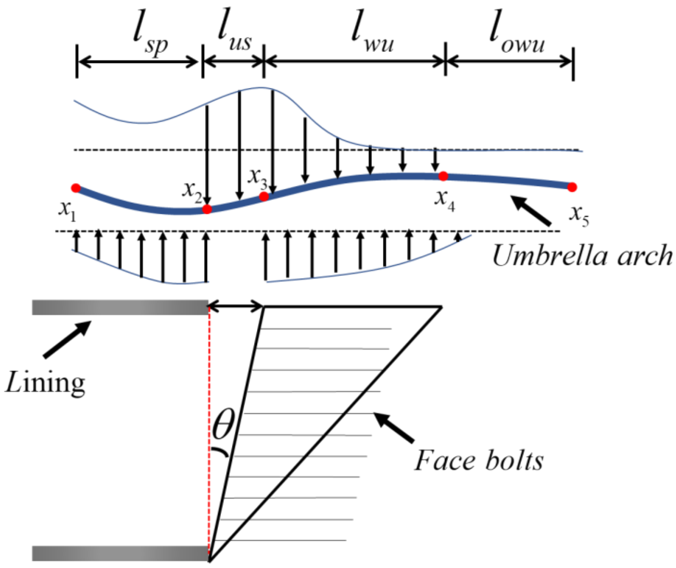

Fig. 7 Case a

b) When the overlap length of the pipe shed is limited ($l_p < x_4 - x_1$). The second situation shown in the **Fig. 8** may occur.

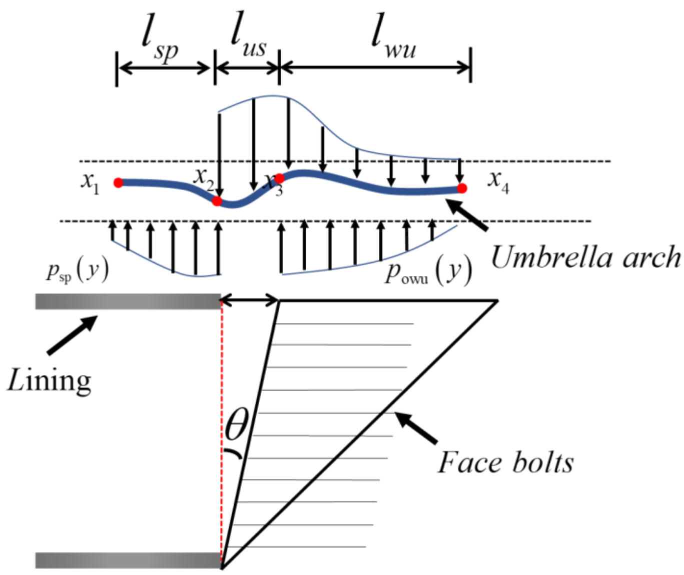

Fig. 8 Case b

$$\sigma_{\text{pipe}} = \frac{d_{\text{pipe}}k_g\int_{l_{sp}+l_{us}}^{l_{sp}+l_{us}+l_{wu}} y_{\text{wu}}(x)\,dx + \left(H\tan(w) - l_{wu}\right)\sigma_{\text{prism}}}{l_{us}+l_{wu}} \tag{53}$$

Further, the minimum density of the face bolt is:

$$n_r = f_{1c} - f_{2c}\frac{c}{H} + f_{3c}\frac{d_{\text{pipe}}k_{\text{g}}\int_{l_{sp}+l_{us}}^{l_{sp}+l_{us}+l_{wu}} y_{\text{wu}}(x)\,\text{dx} + \left(H\tan(w) - l_{wu}\right)\sigma_{\text{prism}}}{H\left(l_{us}+l_{wu}\right)} \tag{54}$$

5 Comparison of results and parameter analysis

5.1 Comparison of results

We focus on discussing and comparing the support pressure required for the inclined tunnel face. Based on analyzing the various possibilities of the inclination angle of the sliding wedge (5°≤w≤70°), the most unfavourable conditions are selected for analysis and verification.

To verify the rationality of the theoretical solution, we compare this paper's solution with Zhao's limit analysis theory (Zhao et al., 2017) and Wen's numerical simulation solution (Wen et al., 2020). In **Fig. 9**, the upper four curves are under the condition of $\gamma H/c$ = 40, and the lower four curves are under the condition of $\gamma H/c$ = 20. The ordinate is the ratio of limit support pressure to cohesion. Comparing three analysis results, they are closely aligned in value, all indicate that the required limit support pressure decreases with an increase in φ. Furthermore, the forward inclination of the excavation face enhances the stability of the tunnel face to some extent.

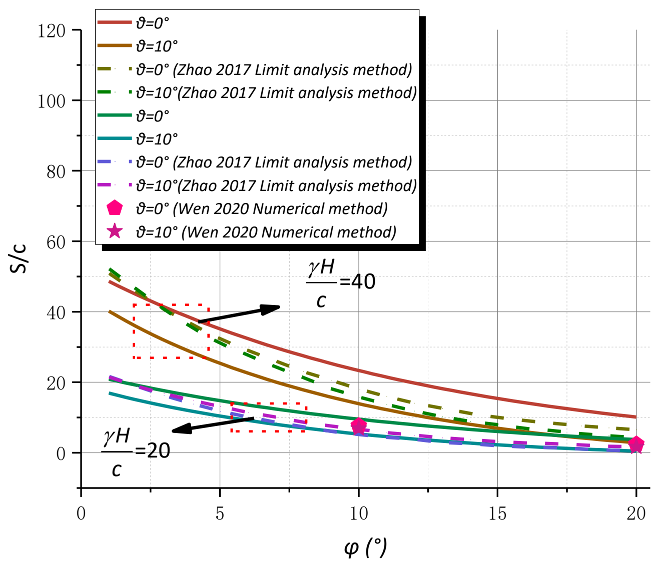

Fig. 9 Relationship between φ and S/c (C/H = 1)

Fig. 10 compares the theoretical solution of the limit support pressure with the limit equilibrium method (Ding et al., 2021) and limit analysis method (Mollon et al., 2009; Mollon et al., 2010; Leca and Dormieux, 1990). As shown in the figure, the limit support pressure calculated by the limit equilibrium method is higher than the upper limit solution of the limit analysis method. Furthermore, the improved model's solution aligns with Ding's research findings. That is, upon implementing advanced pre-reinforcement measures, the required limit support pressure decreases. This reduction is attributed to the ability of the advanced pre-reinforcement to support the vertical load above the excavation face, thereby enhancing its stability.

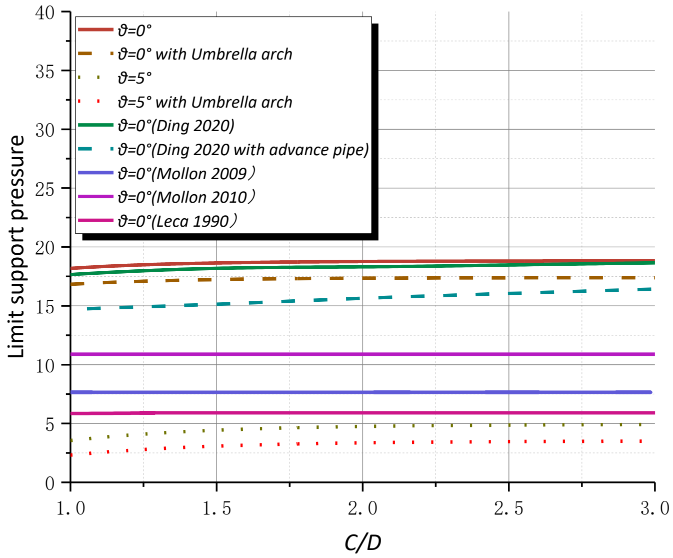

Fig. 10 Relationship between *C/D* and limit support pressure (φ = 25°, c =10kPa, γ =18kN/m^3)

5.2 Parameter analysis

Next, we will discuss the specific influence of stratum and bolt design parameters on the stability of longitudinal inclined tunnel face. The calculation parameters of each case are described in the **Table 1**.

Table 1 Tunnel and stratum parameters

Cases	Height of tunnel *H* (m)	Width of tunnel *B* (m)	Buried depth *C* (m)	Stratum weight γ (kN/m^3)
Fig. 11- Fig. 14	12	10	50	20
Fig. 15- Fig. 16	10	10	50	20

Fig. 11 (a) shows the required minimum bolt density of the middle section of the tunnel under different inclination angles. It can be found that the internal friction angle of the soil has a significant effect on the design of the face bolt. When $\varphi \leq 10°$, the minimum bolt density is much larger than the corresponding value of $\varphi \geq 15°$. In addition, in most cases, the increase of θ can reduce the number of bolts required for the excavation face and improve its stability. This conclusion is consistent with Zhao's theoretical research (Zhao et al., 2017) and Wen's centrifugal test results (Wen et al., 2020). However, the longitudinal inclination angle of tunnel face can not be infinitely increased, which is limited by the maximum unsupported distance. It is worth mentioning that it is not in any case that increasing the inclination angle can effectively lessen the minimum bolt density. As shown in **Fig. 11**(a), when φ = 10°, its curve has an obvious inflection point.

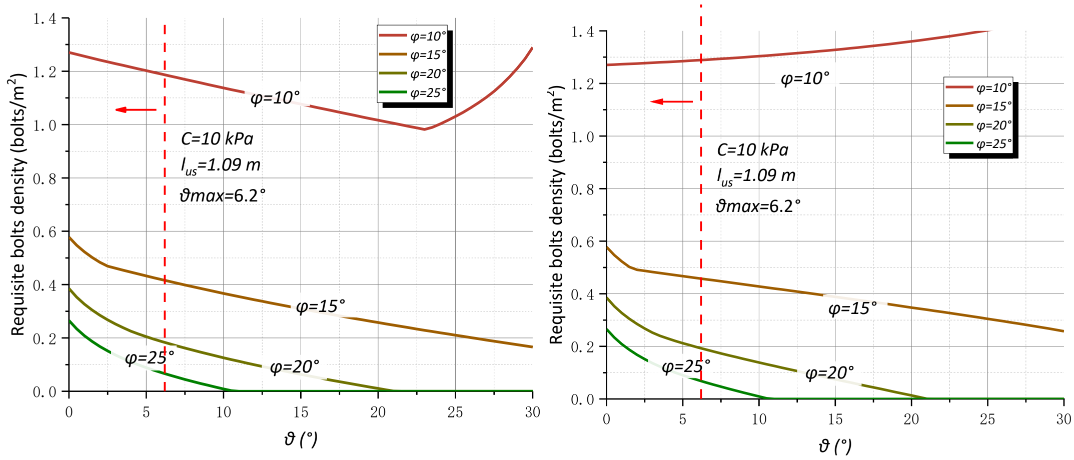

(a) middle section of tunnel (b) exit section of tunnel

Fig. 11 Relationship between φ and n_r (d_{hole} = 114 mm, τ_{max} = 150 kPa, l_{ol} = 12 m)

Different from the middle section of the tunnel, the relation between the inclination angle and the minimum bolt density in the exit section of the tunnel has changed to some extent (**Fig. 11** (b)). Under the condition of the same inclination angle, the minimum bolt density required in the exit section is higher. In addition, when φ = 10°, the stability of the tunnel face is weakened by the forward inclined face. This is due to the fact that the upper stability of the sliding wedge is mainly controlled by the length of the bolt inside the sliding wedge when the friction angle is small. At this time, the forward inclined tunnel face will reduce the effective length of bolt.

Fig. 12 shows that the increase of formation cohesion effectively decreases the bolt density of the tunnel face. This relationship is attributed to the improved mechanical properties of the formation with higher cohesion, leading to a greater maximum inclination angle. Additionally, we found that under deep burial conditions, with the increase of cohesion, the influence of the inclination angle on the stability of the tunnel face diminishes. However, under the condition of shallow burial, although the minimum bolt density is also reduced accordingly with the increase of inclination angle, there is no obvious inflection point in the bolt density curve of the tunnel face at this time.

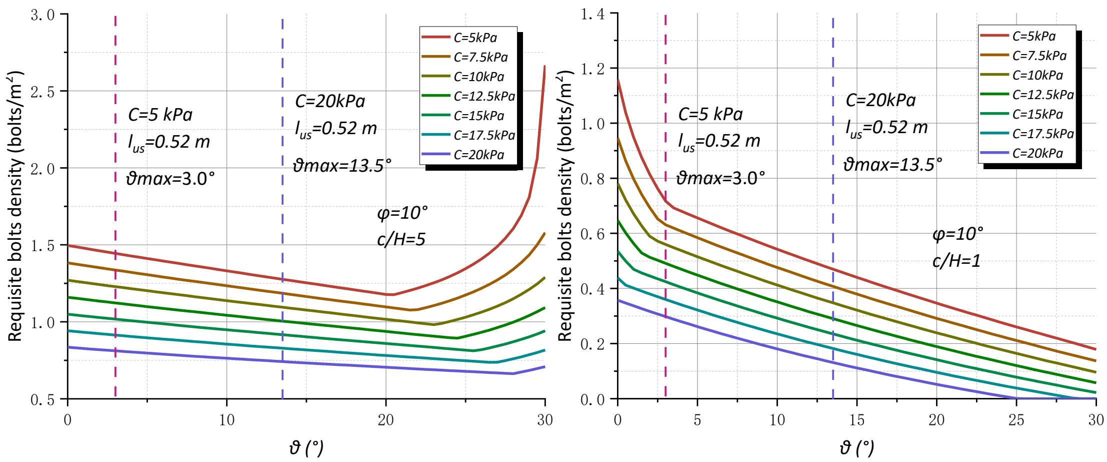

(a) deep tunnel (b) shallow tunnel

Fig. 12 Relationship between c and n_r (middle section of tunnel , φ=10°, d_{hole} = 114 mm, τ_{max} = 150 kPa, l_{ol} = 12 m)

The overlap length of the face bolt is a critical design parameter in the advanced reinforcement method. It determines the maximum excavation length after one round of face bolt reinforcement and the frequency of cyclic application of advanced support bolts. Too short overlap length will make the tunnel face unstable, while too long overlap length will make the material input of the face bolt too much, affecting the construction period. As shown in **Fig. 13**, the required minimum bolt density decreases with the increase of overlap length. However, it is worth mentioning that when its length is greater than 8 m, the effect of increasing length on the minimum bolt density of the tunnel face becomes negligible. This is because, at this time, the stability of the tunnel face has been mainly controlled by the length of the bolt within the sliding wedge, which remains constant once the sliding surface form is established. Therefore, the continued increase in overlap length can be disregarded in terms of its effect on tunnel face stability and bolt forces.

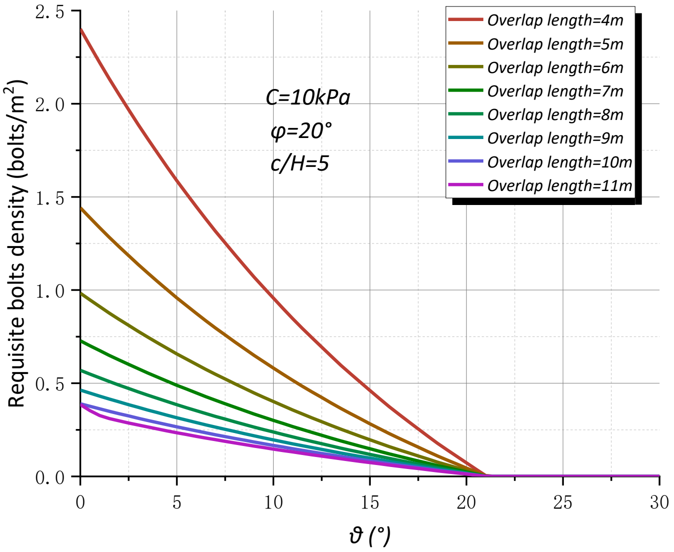

Fig. 13 Relationship between overlap length and n_r (middle section of tunnel, d_{hole} = 114 mm, τ_{max} = 150 kPa)

As shown in **Fig. 14**, the increase in bolt density on the tunnel face is significant to the safety factor of the sliding wedge. However, the increment of the safety factor decreases, which is a concave curve. In addition, it is easy to find that the increase in the inclination angles does not necessarily increase the stability of the tunnel face. When n_r = 0.2, the safety factor decreases with the decrease of θ. However, when the bolt density is large to a certain extent, for example n_r =1, the safety factor of θ = 3° is consistent with the working condition of θ = 5° and is smaller than other inclined angles.

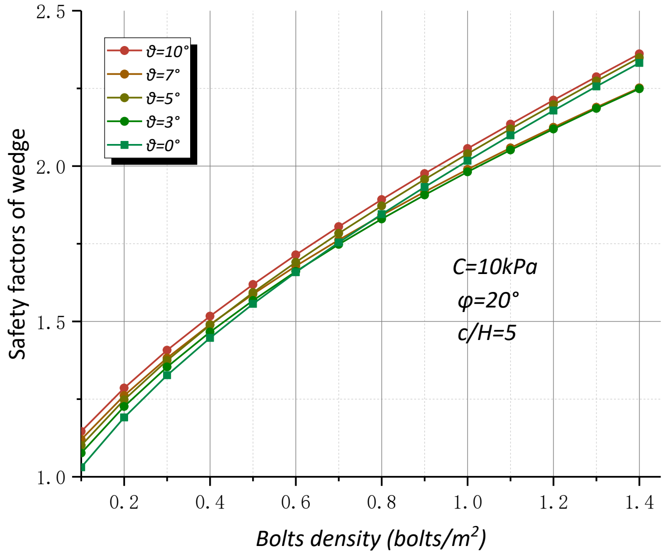

Fig. 14 Relationship between θ and safety factor (middle section of tunnel, d_{hole} = 114 mm, τ_{max} = 150 kPa, l_{ol} = 8 m)

Finally, we discuss the effect of the inclination angle on the stability of the tunnel face after the reinforcement of the pipe shed. As demonstrated in **Fig. 15**, the pipe shed can effectively improve the stability of the excavation face. The specific performance is that the density of the bolt required for the excavation face is reduced. In addition, the adhibition of the pipe shed also changed the law of the lowest density of face bolt, and the two types of curves were not parallel. It is worth mentioning that when φ = 10°, there is a theoretical optimal inclination angle of the tunnel face when there is no pipe shed. However, after the pipe shed reinforcement, there is no obvious inflection point in the minimum density curve of the bolt.

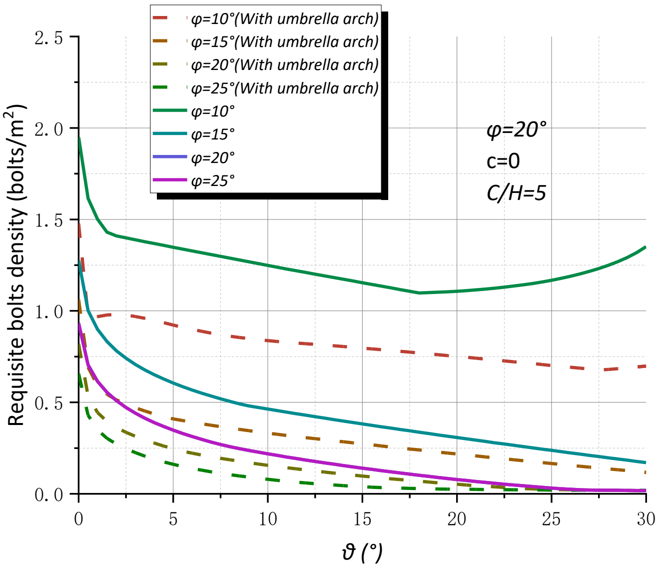

Fig. 15 Relationship between φ and n_r (with or without pipe shed , d_{hole} = 114 mm, τ_{max} = 150 kPa, l_{ol} = 12 m)

From **Fig. 16**, the increase in the pipe shed's overlap length can increase the excavation face's stability to a certain extent. But this increase is limited, especially when the internal friction angle of the stratum is large. This is because the self-stability of the tunnel excavation surface and the soil arch area above it will increase, and the load reduction effect of the pipe shed on the loose area will decrease.

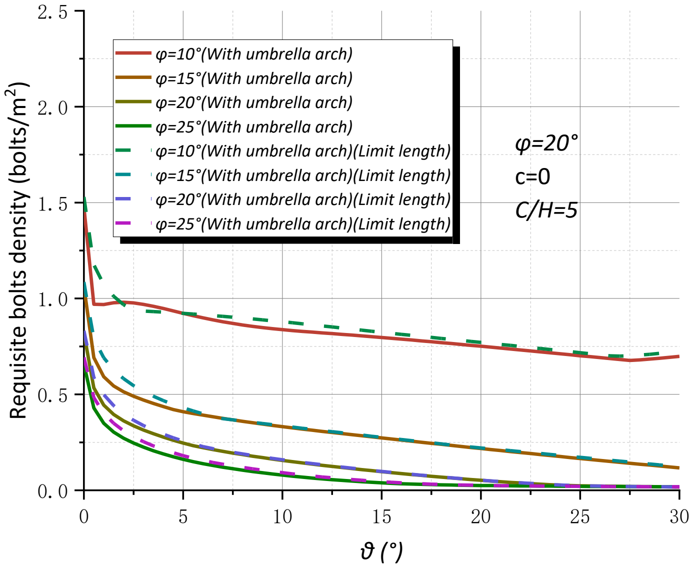

Fig. 16 Relationship between φ and n_r (finite or infinite overlap length of pipe shed, d_{hole} = 114 mm, $\tau_{\max}$ = 350 kPa, l_{ol} = 12 m)

6 Conclusion

This study proposed a stability analysis model considering the shape of the tunnel face and reinforcement measures. The main conclusions are summarized as follows:

(1) According to the limit equilibrium method, a mechanical analysis model is established for a uniquely shaped tunnel face reinforced with horizontal glass fiber bolt.

(2) Taking the longitudinal inclined tunnel face as an example, the calculation formula of the minimum horizontal bolt required for stability in the middle and exit sections of the tunnel is derived.

(3) Based on elastic foundation beam theory, the calculation model of pipe shed-bolt composite pre-reinforcement structure under inclined tunnel face is established, accompanied by the corresponding calculation formula for bolt density.

(4) A forward inclined tunnel face can enhance stability to a certain extent. However, in strata with high cohesion, while the tunnel face may achieve a greater inclination angle, its impact on stability gradually diminishes.

(5) The application of pipe shed can effectively reduce the required minimum bolt density and improve the stability of the tunnel face, especially when the pipe shed overlap length is large.

Acknowledgments

This work is financially supported by the National Natural Science Foundation of China [Grant No. 52108360]. The support is gratefully acknowledged.

Ethics Declaration

Data Availability： Dataset generated is available upon reasonable request and within cooperation agreements.

Declaration of Competing Interest: The authors declare that they have no known competing financial interests or personal relationships that could have appeared to influence the work reported in this paper.

References

Alagha, A. S., & Chapman, D. N. (2019). Numerical modelling of tunnel face stability in homogeneous and layered soft groun. *Tunnelling and Underground Space Technology*, 94(12), 1030. https://doi.org/10.1016/j.tust.2019.103096.

Anagnostou, G., & Kovári, K. (1996). Face stability conditions with earth-pressure-balanced shields. *Tunnelling and underground space technology*, 11(2), 165-173. https://doi.org/10.1016/0886-7798(96)00017-X.

Anagnostou, G., & Serafeimidis, K. (2007). The dimensioning of tunnel face reinforcement. Underground Space–the 4th Dimension of Metropolises. ITA World Tunnel Congress, Prague, 291-296.

Anagnostou, G., & Perazzelli, P. (2013) The stability of a tunnel face with a free span and a non-uniform support. *Geotechnik*, 36(1), 40-50. https://doi.org/10.1002/gete.201200014.

Anagnostou, G., & Perazzelli, P. (2015). Analysis method and design charts for bolt reinforcement of the tunnel face in cohesive-frictional soils. *Tunnelling and Underground Space Technology*, 47(3), 162-81. https://doi.org/10.1016/j.tust.2014.10.007.

Chambon, P., & Corte, J.F. (1994). Shallow tunnels in cohesionless soil: stability of tunnel face. *Journal of Geotechnical Engineering*, 120(7), 1148-1165.https://doi.org/10.1061/(ASCE)0733-9410(1994)120:7(1148).

Ding, W., Wang, H., Liu, K., et al. (2021). Stability Evaluation Model of a Tunnel Face Excavated by the Benching Method in a Soft Silty Clay Layer. *International Journal of Geomechanics*, 21(4), 04021022. https://doi.org/10.1061/(ASCE)GM.1943-5622.0001962.

Ding, X., Weng, Y., Zhang, Y., Xu, T., Wang, T., Rao, Z., & Qi, Z. (2017). Stability of large parallel tunnels excavated in weak rocks: a case study. *Rock Mechanics and Rock Engineering*, 50, 2443-2464. https://doi.org/10.1007/s00603-017-1247-6.

Guan, B.S., & Zhao, Y. (2011). Construction technology of weak surrounding rock tunnel. People 's Transportation Publishing Hous.

Huang, Q., Zou, J.F., Qian, Z.H. (2019). Face stability analysis for a longitudinally inclined tunnel in anisotropic cohesive soils. *Journal of Central South University*, 26(7), 1780-1793. https://doi.org/10.1007/s11771-019-4133-4.

Kirsch, A. (2010). Experimental investigation of the face stability of shallow tunnels in sand. *Acta Geotechnica*, 5(1), 43-62. https://doi.org/10.1007/s11440-010-0110-7.

Leca, E., Dormieux, L. (1990). Upper and lower bound solutions for the face stability of shallow circular tunnels in frictional material. *Geotechnique*, 40(4),581-606. https://doi.org/10.1680/geot.1990.40.4.581.

Li, B., Hong, Y., Gao, B., et al. (2015). Numerical parametric study on stability and deformation of tunnel face reinforced with face bolts. *Tunnelling and Underground Space Technology*, 47: 73-80. https://doi.org/10.1016/j.undsp.2023.10.002.

Mollon, G., Dias, D., Soubra, A.H. (2009). Probabilistic analysis and design of circular tunnels against face stability. *International Journal of Geomechanics*, 9(6), 237-49.

https://doi.org/10.1061/(ASCE)1532-3641(2009)9:6(237).

Mollon, G., Dias, D., Soubra, A.H. (2010). Face stability analysis of circular tunnels driven by a pressurized shield. *Journal of Geotechnical and Geoenvironmental Engineering*, 136(1), 215-29. https://doi.org/10.1061/(ASCE)GT.1943-5606.0000194.

Murayama, S., Endo, M., Hashiba, T., Yamamoto, K., Sasaki, H. (1966). Geotechnical aspects for the excavating performance of the shield machines. The 21st annual lecture in meeting of Japan Society of Civil Engineers 265.

Oreste, P., Dias, D. (2012). Stabilisation of the excavation face in shallow tunnels using fibreglass dowels. Rock mechanics and rock engineering, 45(4), 499-517. https://doi.org/10.1007/s00603-012-0234-1.

Oreste, P. (2009).The dimensioning of dowels for the stabilization of potentially unstable rock blocks on the walls of underground chambers. *Geotechnical and Geological Engineering*, 27(1), 53-69. https://doi.org/10.1007/s10706-008-9211-6.

Pan, Q., Dias, D. (2017). Upper-bound analysis on the face stability of a non-circular tunne. *Tunnelling and Underground Space Technology*, 62, 96-102. https://doi.org/10.1016/j.tust.2016.11.010.

Ranjbarnia, M., Fahimifar, A., Oreste, P. (2016). Practical method for the design of pretensioned fully grouted rockbolts in tunnels. *International Journal of geomechanics*, 16(1), 04015012. https://doi.org/10.1061/(ASCE)GM.1943-5622.0000464.

Takano, D., Otani, J., Nagatani, H., et al. (2006). Application of x-ray CT on boundary value problems in geotechnical engineering: research on tunnel face failure. GeoCongress 2006: Geotechnical Engineering in the Information Technology Age, 1-6. https://doi.org/10.1061/40803(187)50.

Terazaghi, K. (1965) Theoretical soil mechanics. John Wiley and Sons.

Ukritchon, B., Keawsawasvong, S. (2017). Design equations for undrained stability of opening in underground walls. *Tunnelling and Underground Space Technology*, 70(11), 214-20. https://doi.org/10.1016/j.tust.2017.08.004.

Vermeer, P.A., Ruse, N., Marcher, T. (2002). Tunnel heading stability in drained ground. Felsbau 20(6):8-18.

Wang, Z., Wang, Y., Wang, S., et al. (2020). Effect of Longitudinal Gradient on 3D Face Stability of Circular Tunnel in Undrained Clay. *Advances in Civil Engineering*, 2021(2), 1-14. https://doi.org/10.1155/2020/5846151.

Weng, X., Sun, Y., Yan, B., et al. (2020). Centrifuge testing and numerical modeling of tunnel face stability considering longitudinal slope angle and steady state seepage in soft clay. *Tunnelling and Underground Space Technology*, 101, 103406. https://doi.org/10.1016/j.tust.2020.103406.

Zhang, X., Wang, M., Lyu, C., et al. (2022). Experimental and numerical study on tunnel faces reinforced by horizontal bolts in sandy ground. *Tunnelling and Underground Space Technology*, 123,104412. https://doi.org/10.1016/j.tust.2022.104412.

Zhang, X., Wang, M., Wang, Z., et al. (2020). Stability analysis model for a tunnel face reinforced with bolts and an umbrella arch in cohesive-frictional soils. *Computers and Geotechnics*, 124(8), 103635. https://doi.org/10.1016/j.compgeo.2020.103635.

Zhao, L., Li, D., Li, L., et al. (2017). Three-dimensional stability analysis of a longitudinally inclined shallow tunnel face. *Computers and Geotechnics*, 87(7), 32-48. https://doi.org/10.1016/j.compgeo.2017.01.015.

Appendix I

$$\Lambda = \frac{2\lambda \tan\varphi}{\cos\omega - \sin\omega \tan\varphi} \tag{1}$$

$$M = M_c B^2 c - M_\gamma B^3 \gamma \tag{2}$$

$$M_c = \frac{\Lambda \tan\omega}{\lambda \tan\varphi} \tag{3}$$

$$M_\gamma = \tan\omega \tag{4}$$

$$P = P_c B^2 c + P_s B^2 s \tag{5}$$

$$P_c = \frac{\Lambda}{2\lambda \tan\varphi \cos\omega} \tag{6}$$

$$P_s = \tan(\varphi + w) \tag{7}$$

$$C_v = e^{(\Lambda H/B)} \tag{8}$$

$$F = C_v - 1 - \frac{\Lambda H}{B} \tag{9}$$

Appendix II

Through the Winkler beam model, the mechanical equations of different characteristic sections of the pipe shed are established. Then the general deflection solutions of different characteristic sections on the pipe shed can be solved (Zhang et al., 2020). Specifically:

$$y_{sp}(x) = e^{\beta_1 x}\left(\alpha_1 \cos\beta_1 x + \alpha_2 \sin\beta_1 x\right) + e^{-\beta_1 x}\left(\alpha_3 \cos\beta_1 x + \alpha_4 \sin\beta_1 x\right) \tag{1}$$

$$y_{us}(x) = \frac{l_p \sigma_{vn}}{24 E_2 I_2} x^5 + \alpha_5 x^3 + \alpha_6 x^2 + \alpha_7 x + \alpha_8 \tag{2}$$

$$\begin{aligned} & y_{wu}(x) = e^{\beta_2 x}\left(\alpha_9 \cos\beta_2 x + \alpha_{10} \sin\beta_2 x\right) \\ & + e^{-\beta_2 x}\left(\alpha_{11} \cos\beta_2 x + \alpha_{12} \sin\beta_2 x\right) \\ & + \frac{l_p \sigma_{vn}}{k_{wu} d_{pipe}}\left[1 - \cosh\beta_2 (x - x_4) \cos\beta_2 (x - x_4)\right] \end{aligned} \tag{3}$$

$$y_{owu}(x) = e^{\beta_2 x}\left(\alpha_9 \cos\beta_2 x + \alpha_{10} \sin\beta_2 x\right) + e^{-\beta_2 x}\left(\alpha_{11} \cos\beta_2 x + \alpha_{12} \sin\beta_2 x\right) \tag{4}$$

Where

$$
\begin{aligned}
\beta_1 &= \sqrt[4]{\frac{k_{sp} d_{pipe}}{4E_2 I_2}} \\
\beta_2 &= \sqrt[4]{\frac{k_{wu} d_{pipe}}{4E_2 I_2}}
\end{aligned} \tag{5}
$$

In order to solve the 12 undetermined coefficients, the following boundary conditions need to be passed:

(1) The left end of the pipe shed is usually welded on the steel arch, so the first moment of displacement and displacement here is 0, that is :

$$
\begin{aligned}
y_{sp}(x_1) &= 0 \\
y'_{sp}(x_1) &= 0
\end{aligned} \tag{6}
$$

(2) The strain at the intersection of the pipe sheds of different characteristic sections is continuous, the shear force is equal, and the bending moment is equal, that is :

$$
\begin{aligned}
y_{sp}(x_2) &= y_{us}(x_2) \\
y'_{sp}(x_2) &= y'_{us}(x_2) \\
y''_{sp}(x_2) &= y''_{us}(x_2) \\
y'''_{sp}(x_2) &= y'''_{us}(x_2) \\
y_{us}(x_3) &= y_{wu}(x_3) \\
y'_{us}(x_3) &= y'_{wu}(x_3) \\
y''_{us}(x_3) &= y''_{wu}(x_3) \\
y'''_{us}(x_3) &= y'''_{wu}(x_3)
\end{aligned} \tag{7}
$$

(3) At the free end of the pipe shed, although it can be freely deformed, its shear force and bending moment are 0, that is :

$$
\begin{aligned}
y''_{owu}(x_5) &= 0 \\
y'''_{owu}(x_5) &= 0
\end{aligned} \tag{8}
$$